Research Article Vol. 33, No. 5 / 10 Mar 2025 / Optics Express 10873
Optics EXPRESS

Study and mitigation of polarization fading in FBG-assisted direct-detection φ-OTDR

FOURIER SANDAH,[1,2,*] MICHEL DOSSOU,[2] DAMIEN KINET,[1] PRASAD DANDU,[1] AND MARC WUILPART[1]

[1] Unit of Electromagnetism and Telecommunications, University of Mons, Boulevard Dolez 31, 7000, Mons, Belgium
[2] Research Unit in Photonics and Wireless Communications, LETIA/EPAC, University of Abomey-Calavi, 01 BP 526, Abomey-Calavi, Benin
[*] beni.sandah@umons.ac.be

Abstract: In this paper, the detrimental polarization effects in direct detection fiber Bragg grating (FBG)-assisted phase-OTDR sensing systems are investigated. The detrimental effects result from a mismatch between the states of polarization reflected by two successive FBGs. A numerical analysis is first performed to quantify the polarization dependence of the sensor response. It is shown that the use of standard single-mode and polarization-maintaining fibers could present a non-negligible polarization dependence. The mitigation of the polarization effect when using spun fibers is also quantified. Second, an experimental setup allowing the measurement of the polarization dependence of the sensor response is proposed, and results obtained for standard single-mode, polarization maintaining, and spun fibers are presented. The results showed a good agreement with the numerical data.

1. Introduction

Over the past decade, phase optical time-domain reflectometry (φ-OTDR) has garnered considerable attention due to its extensive potential in sensing applications. This technique involves transmitting an optical pulse generated by a narrow linewidth laser (NLL) through an optical fiber and measuring the Rayleigh-backscattered signal as a function of time. Using an NLL enables the detected power to become sensitive to the phase difference between the signals backscattered by the scattering centers within the resolution length (half the pulse width). Consequently, any external perturbation that locally modifies the refractive index or/and elongates the fiber will result in a change in the recorded backscattered power at the perturbation location. In particular, phase-ODTR systems have been applied for vibration localization [1], intrusion sensing [2], detection of seismic waves [3] and railways monitoring [4].

A primary challenge in applying φ-OTDR to standard optical fibers is the low signal-to-noise ratio (SNR) due to the weak power level of Rayleigh backscattering. To improve the signal reception, several techniques, including signal processing [5], and amplification [6] have been explored. An alternative method involves using specialty fibers to enhance backscattered power either in a distributed [7] or quasi-distributed scheme [8]. One of the quasi-distributed enhancement approaches includes integrating arrays of identical weak fiber Bragg gratings (FBGs) in the sensing fiber. The fundamental concept of the so-called FBG-assisted phase-OTDR involves analyzing the interference signal created by the waves reflected by two consecutive FBGs. This interference signal can be detected on the φ-OTDR trace if the distance between two successive FBGs is smaller than the resolution length [9,10]. Any disturbance occurring between two successive FBGs will lead to a change in the phase difference between the two reflected waves, thus modifying the power recorded at the interference signal position on the φ-OTDR trace.

#549916 https://doi.org/10.1364/OE.549916
Journal © 2025 Received 25 Nov 2024; revised 18 Jan 2025; accepted 31 Jan 2025; published 3 Mar 2025

Optics EXPRESS

Interrogating a series of identical FBGs increases the SNR but also introduces some undesirable effects such as spectral shadowing, multi-reflection crosstalk (MRC), and polarization effects. When spectral shadowing occurs, crosstalk may appear. A technique is proposed in [11], to alleviate the spectral shadowing for single pulse FBG-assisted phase-OTDR. When the distances between two successive FBGs are identical, MRC between FBGs becomes critical as described in [12].

The interference of the signals reflected by two consecutive FBGs is also subject to detrimental polarization effects as the fiber exhibits some birefringence. The states of polarization (SOPs) of the interfering signals do not necessarily align (polarization mismatch), leading to a polarization fading phenomenon. In extreme cases, this fading can be complete, rendering the sensor unresponsive to external disturbances (such as vibrations). To the best of the authors' knowledge, the fading polarization effect has yet to be thoroughly examined within the context of FBG-assisted direct-detection φ-OTDR systems. In the literature, it is assumed that the propagation medium exhibits a weak birefringence [9,10] or it is proposed to perform the measurement for two different orhtogonal SOPs [13]. This last approach allows reducing the polarization fading but does not necessarily provide the best sensitivity.

Note that the polarization properties of light have been studied in the scope of φ-OTDR in other contexts. For instance, in [14], the detection of audio signals and footsteps using a polarization-multiplexed coded differential φ-OTDR interrogation of standard telecom fibers was proposed. This study focused on the use of polarization diversity and coherent detection.

In the first part of the work, a numerical analysis to study the polarization fading effect for direct detection FBG-assisted φ-OTDR sensors is proposed. A parameter, the polarization fading sensitivity (PFS), is first defined to quantify the polarization dependence of the sensor's performance. The PFSs of unspun and spun fibers are then determined by simulation. A uniformly spun fibre (SF) is a speciality fibre produced by rotating or spinning a linearly birefringent fibre preform about its axes at a constant spin rate during the standard fibre drawing process with a constant spin rate ξ (in rad/m). This spinning helps to reduce the global birefringence, making spun fibers good candidates for mitigating polarization fading in FBG-assisted φ-OTDR. Two kinds of unspun fibers have been considered: a single mode fiber (SMF) for which the length is much smaller than the coupling length [15] and a polarization-maintaining fiber (PMF) [16]. In the second part of the work, an experimental setup is proposed to measure the PFS for SMF, PMF, and SF. Experimental results are described and compared with those of the numerical analysis. Note that the polarization fading can be removed by a polarization diversity receiver [17,18]. For instance, in [19], exploiting both polarization diversity through delayed polarization multiplexing and an aperiodic autocorrelation of a pseudorandom binary sequence enabled the mitigation of polarization fading to give a polarization-independent phase variation induced by an applied vibration. Nevertheless, the porlarization diversity approach, requiring a coherent detection scheme, is not adequate in our study since we focused on direct detection φ-OTDRs. Direct detection is still preferred when the sensing system involves low-cost lasers. For instance, if the sensing system is used to monitor a passive optical network (PON) [20], already installed DBF (distributed feed-back) sources could be used to reduce the cost. Since a typical value for the coherence length of DBF lasers about 20 m (corresponding to 3 MHz linewidth), and a PON maximum distance is 20 km, it is not adequate to use a coherent detection scheme.

2. FBG-assisted φ-OTDR principle

The fundamental concept of FBG-assisted φ-OTDR is presented in Fig. 1(a), which focuses on a specific pair of two consecutive FBGs (FBG_A and FBG_B) inscribed along the sensing fiber. The distance between the FBGs is denoted by L_F. The NLL emits pulses with a width W, ensuring that $\frac{W}{2} - L_F > 0$ [11]. Under these circumstances, the resultant φ-OTDR trace exhibits a three-level characteristic as seen in Fig. 1(b). The power levels P_A and P_B correspond to the waves reflected

Optics EXPRESS

by FBG_A and FBG_B, respectively, whereas P_{AB} denotes the power observed in the interference zone (arising from the combination of the waves reflected by FBG_A and FBG_B). When a vibration is introduced between FBG_A and FBG_B, P_{AB} will fluctuate over time. A frequency analysis of $P_{\mathrm{AB}}(t)$ enables the determination of the local vibration characteristics. $P_{\mathrm{AB}}(t)$ can be obtained by analyzing phase-OTDR traces measured at a specified repetition rate. Let us define ΔP as the power difference between the maximum and the minimum P_{AB} detected over time (see Fig. 1(b)). The larger ΔP, the higher the sensitivity of the sensor to a given perturbation. Note that in Fig. 1, the Rayleigh backscattering level has not been represented since it is assumed to be much smaller than the reflected powers.

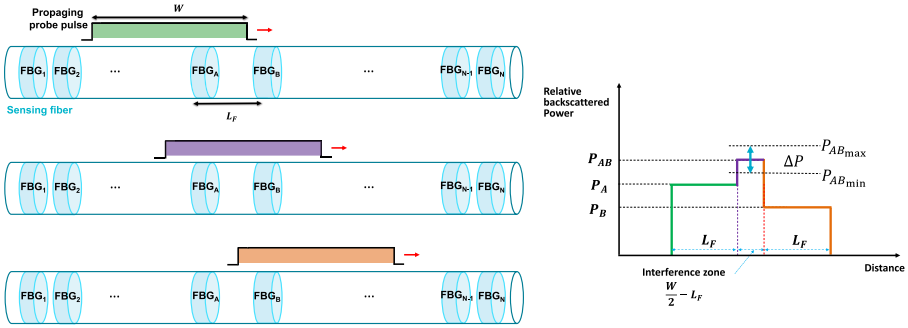

Fig. 1. (a) Principle of the interaction between the interrogating pulse and two consecutive FBGs, (b) typical φ-OTDR signal for two consecutive FBGs

3. Simulation of polarization fading

The efficiency of the interference effect leading to $P_{\mathrm{AB}}(t)$ depends on the SOPs of the two reflected waves. Any polarization mismatch that may arise when the propagation medium between the FBGs is birefringent will degrade the interference efficiency. In the ideal case of no birefringence, there is no polarization mismatch, ΔP is the largest and the sensor offers an optimal sensitivity. When birefringence cannot be neglected, the reflected waves P_A and P_B will be characterized by two different SOPs resulting in a polarization fading. When the two SOPs are orthogonal, the two reflected waves no longer interfere and P_{AB} becomes insensitive to the external perturbation ($\Delta P = 0$). Clearly, this situation should be avoided to ensure a good operation of the sensor.

The sensitivity of FBG-assisted φ-OTDR systems to polarization fading effect can be quantified by the polarization fading sensitivity (PFS) parameter, defined as:

$$\mathrm{PFS} = 10 \log \frac{\Delta P_{\max}}{\Delta P_{\min}} \tag{1}$$

where $\Delta P_{max(min)}$ is the maximum (minimum) value of ΔP over all the possible SOPs at the input of FBG_A and for a given perturbation. A PFS of 0 dB means that the sensor does not present any sensitivity to polarization effects. The worst case is obtained when the PFS shows an infinite value. This is obtained when $\Delta P_{\min} = 0$, i.e. there exists an input SOP so that the two interfering signals have orthogonal polarizations.

In the presence of birefringence, ΔP depends on the SOPs of the two reflected complex electric fields $\boldsymbol{E_A}$ and $\boldsymbol{E_B}$, which are a function of the input SOP and the birefringence properties of the fiber. The Jones formalism [21] was used to determine ΔP as a function of the input SOP and the birefringence parameters. When modeling the polarization effects, the x and y components of the

Optics EXPRESS

electric field have to be considered. P_{AB} is therefore given by:

$$P_{\mathrm{AB}} = |\boldsymbol{E_{A,x}} + \boldsymbol{E_{B,x}}|^2 + |\boldsymbol{E_{A,y}} + \boldsymbol{E_{B,y}}|^2 \tag{2}$$

where $E_{A(B),x}$ and $E_{A(B),y}$ are the x and y components of the input complex electric field reflected by $\mathrm{FBG}_{A(B)}$ and reaching the OTDR unit, respectively. They can be calculated as:

$$\begin{pmatrix} \boldsymbol{E_{A,x}} \\ \boldsymbol{E_{A,y}} \end{pmatrix} = \mathbf{M_L^T M_{RA} M_L} \begin{pmatrix} \boldsymbol{E_{in,x}} \\ \boldsymbol{E_{in,y}} \end{pmatrix} e^{-\alpha z_A} e^{j\frac{4\pi}{\lambda} n z_A} \tag{3}$$

$$\begin{pmatrix} \boldsymbol{E_{B,x}} \\ \boldsymbol{E_{B,y}} \end{pmatrix} = \mathbf{M_L^T M_{RA} M_F^T M_{RB} M_F M_{TA} M_L} \begin{pmatrix} \boldsymbol{E_{in,x}} \\ \boldsymbol{E_{in,y}} \end{pmatrix} e^{-\alpha z_B} e^{j\frac{4\pi}{\lambda} n z_B} \tag{4}$$

where $\mathbf{E_{in,x}}$ and $\mathbf{E_{in,y}}$ are the x and y components of the input complex electric field. $\mathbf{M_{TA}}$ is the Jones matrix of FBG_A in transmission and $\mathbf{M_{Ri}}$ ($i = A; B$) is the Jones matrix of FBG_i in reflection. α is the fiber linear attenuation expressed in m^{-1} and $z_{A(B)}$ is the distance between the fiber input and the first (second) FBG. $\mathbf{M_L}$ is the forward Jones matrix of the lead fiber, i.e., the fiber section placed between the φ-OTDR unit and FBG_A. $\mathbf{M_F}$ is the forward Jones matrix of the fiber section placed between the FBGs. The backward propagations through the lead fiber and the fiber section between FBG_A and FBG_B are represented by the transpose of the forward matrices (denoted by $^{\mathbf{T}}$ in Eq. (3) and (4)). This implies that only reciprocal birefringence effects are taken into account [22]. Only the presence of a strong axial magnetic field will make this assumption incorrect [23]. The input normalized Jones vector field can be represented by [24]:

$$\begin{pmatrix} \boldsymbol{E_{in,x}} \\ \boldsymbol{E_{in,y}} \end{pmatrix} = \begin{pmatrix} \cos\varphi\cos\chi - j\sin\varphi\sin\chi \\ \sin\varphi\cos\chi + j\cos\varphi\sin\chi \end{pmatrix} \tag{5}$$

where φ and χ are the azimuth and ellipticity angles of the input SOP. In general, the SOP at the input of a pair of two successive FBGs is unknown so that φ and χ can take any values in the ranges $[0, \pi]$ and $\left[-\frac{\pi}{4}, \frac{\pi}{4}\right]$, respectively. Since Eq. (5) corresponds to the normalized Jones vector, P_{AB} obtained from Eq. (2) is a power normalized with respect to the input power. As identical FBGs have been used in the case of this study, we have $\mathbf{M_{RA}} = \mathbf{M_{RB}} = \mathbf{M_R}$. $\mathbf{M_R}$ ($\mathbf{M_{TA}}$) corresponds to the multiplication of the complex reflection (transmission) coefficient $\mathbf{r}$ ($\mathbf{t}$) by a 2 $\times$ 2 unitary diagonal matrix. $\mathbf{r}$ and $\mathbf{t}$ can be defined as [25]:

$$\mathbf{r} = \frac{-\kappa \sinh(\alpha_c L_{FBG})}{\hat{\sigma}\sinh(\alpha_c L_{FBG}) + j\alpha_c \cosh(\alpha L_{FBG})} \tag{6}$$

$$\mathbf{t} = \frac{j\alpha}{\hat{\sigma}\sinh(\alpha_c L_{FBG}) + j\alpha_c \cosh(\alpha_c L_{FBG})} \tag{7}$$

where:

$$\hat{\sigma} = \delta + \sigma,\ \kappa = \frac{\pi}{\lambda}\nu\delta_n\ ,\ \alpha_c = \sqrt{\kappa^2 - \hat{\sigma}^2}\ ,\ \delta = \frac{2\pi n_{\mathrm{eff}}}{\lambda} - \frac{\pi}{\Lambda}\ ,\ \sigma = \frac{2\pi}{\lambda}\delta_n$$

with κ the mode coupling factor of the propagating modes, $\hat{\sigma}$ the auto-coupling coefficient of the propagating modes, δ the decoupling factor, δ_n the variation of the refractive index in the Bragg grating and ν the visibility of the grating. Note that the birefringence of the FBGs was neglected since the x and y components see the same $\mathbf{r}$ and $\mathbf{t}$ coefficient. This is in agreement with the experimental study since very low reflective FBGs were considered (see section 5). The $\mathbf{M_F}$ matrix in Eq. (4) is influenced by the type of fiber located between the FBGs. For the purposes of this study, both unspun and spun fibers are considered. The specific feature of a

Optics EXPRESS

spun fiber is its spun period $S_P = 2\pi/\xi$ where ξ is the spin rate [26]. The efficiency of the global birefringence reduction is higher when the spun period S_P is smaller (i.e. when ξ is higher). The Jones matrix of a spun fiber of length L_F can be obtained by concatenating two Jones matrix elements: a retarder $\mathbf{R}$ and a rotator $\mathbf{\Omega}$ as [27]:

$$\mathbf{M_F} = \mathbf{\Omega R} \tag{8}$$

where

$$\mathbf{R} = \begin{pmatrix} \cos\frac{R(z)}{2} + j\sin\frac{R(z)}{2}\cos 2\phi(z) & j\sin\frac{R(z)}{2}\sin 2\phi(z) \\ j\sin\frac{R(z)}{2}\sin 2\phi(z) & \cos\frac{R(z)}{2} - j\sin\frac{R(z)}{2}\cos 2\phi(z) \end{pmatrix} \tag{9}$$

$$\mathbf{\Omega} = \begin{pmatrix} \cos\Omega(z) & -\sin\Omega(z) \\ \sin\Omega(z) & \cos\Omega(z) \end{pmatrix} \tag{10}$$

with the retardation $R(z)$, its principle axis orientation $\phi(z)$, and the rotation $\Omega(z)$ in forward and backward directions written as:

$$R(z) = 2\,sin^{-1}\left(\frac{1}{(1+q^2)^{1/2}} sin\,\gamma z\right) \tag{11}$$

$$\Omega(z) = \xi z + tan^{-1}\left(\frac{-q}{(1+q^2)^{1/2}} tan\,\gamma z\right) + n\pi \tag{12}$$

$$\phi(z) = \frac{\xi z - \Omega(z)}{2} + \frac{m\pi}{2} + q_0 \tag{13}$$

where m and n are integers, $z = L_F$ is the distance between the two consecutive FBGs, q_0 is the initial orientation (at $z = 0$) of the local slow axis. The parameters q and γ_L are defined as followed:

$$q = \frac{2(\xi + f_m)}{\Delta\beta}\ ;\ \gamma = \frac{1}{2}\sqrt{\Delta\beta^2 + 4(\xi + f_m)^2} \tag{14}$$

where $\Delta\beta$ represents the linear birefringence of the fiber (equal to $\Delta\beta = 2\pi/L_B$ where L_B is the beat length). f_m is the Faraday-induced rotation angle per unit length. $f_m = 0$ when the fiber is not subjected to a longitudinal magnetic field, which is the case in this work. Equation (8) will be used to simulate the polarization effects in unspun ($\xi = 0$) and spun fibers ($\xi \neq 0$).

For the simulation of polarization effects in a dynamic case (when vibrations are applied), we will consider that the effect of vibration is to induce a local variation of the fiber length (dynamic elongation). This situation corresponds to the experimental arrangement described in section 5 (use of a piezo transducer to induce a perturbation). To take into account polarization effects while perturbing the fiber between the gratings, the length L_F expressed in $\mathbf{M_F}$ and $\mathbf{M_F^T}$ (defined in Eq. (8)) becomes time-dependent with:

$$L_F(t) = L_{F0} + \Delta L_{\max}\cos(2\pi f t) \tag{15}$$

where $\Delta L_{\max}$ is the maximum amplitude of length variation and L_{F0} is the fiber length when no vibration is applied between FBGs.

To calculate the PFS, the simulator first calculates the time variation of $P_{\mathrm{AB}}(t)$ for every pair of (φ, χ) using Eq. (5) to (15). For every (φ, χ) pair, ΔP can be calculated. When all the input SOPs are swept, ΔP maximum and ΔP minimum can be determined, as well as the PFS using Eq. (1).

Optics EXPRESS

4. Simulation results

4.1. Unspun fibers case

The case of unspun fibers ($\xi = 0$) was first investigated. Using the simulation procedure described in section 3, the power variation ΔP for a vibration strength $\Delta L_{\max} = 1.68 \times 10^{-7}$ m was calculated as a function of the input SOP (with a $\frac{\pi}{128}$ step for both φ and χ). The $\Delta L_{\max}$ value was chosen based on the vibration parameters used in experiments: $\Delta L_{\max} = K_{\text{str}} V_{\text{pp}}$ with $K_{\text{str}} = 3.6$ μm/V (the fiber stretch coefficient of the PZT transducer) and $V_{\text{pp}} = 44$ mV (peak-to-peak voltage applied to the PZT by the function generator). The calculation of the normalized ΔP (with respect to the input power) as a function of φ and χ for three different beat lengths L_B was carried out and is presented in Fig. 2. The largest ($\Delta P_{\max}$) and the smallest ($\Delta P_{\min}$) value of ΔP can then be used to calculate the PFS. When the reflected SOPs are orthogonal for $L_F = L_{F0}$ as presented in Fig. 2(a) ($q_0 = 0$, $\varphi = \pi/4$, $\chi = 0$, $L_B = 4L_{F0}$ and $L_{F0} = 40$ m), the PFS reaches a high value (PFS = 86 dB). $L_F = 40$ m was chosen as it is close to the distance between the FBGs used in experiments. On the contrary, when the SOPs are aligned for every input SOP (case of no birefringence $\Delta\beta = 0, L_B = \infty$), ΔP remains identical for all the (φ, χ) pair and the PFS is equal to zero as shown in Fig. 2(b). Another intermediate example is shown in Fig. 2(c) for $L_B = 3$ m (order of magnitude for the SMF fiber coiled around a piezo-transducer, see section 5), the calcultated PFS is equal to 5 dB.

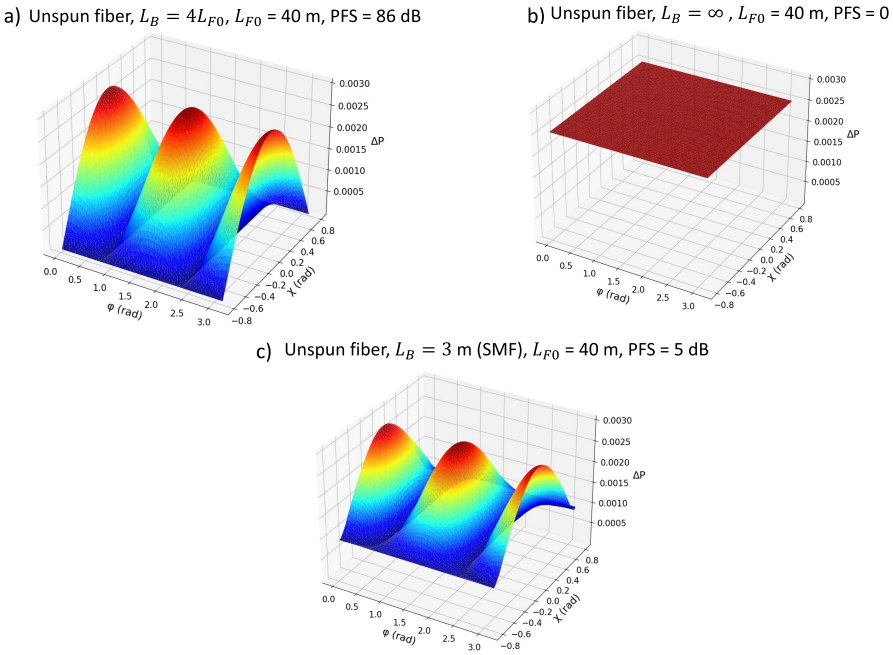

Fig. 2. ΔP as a function of the input SOP (ϕ and χ) for an unspun fiber with $L_{F0} = 40$ m and $\Delta L_{\max} = 1.68 \times 10^{-7}$ m: (a) $L_B = 4L_{F0}$, (b) $L_B = \infty$ and (c) $L_B = 3$ m.

Figure 3 presents the evolution of the PFS as function of L_{F0}/L_B for a distance changing from 3 to 45 m, and with $L_B = 3$ m. The L_{F0}/L_B ratio therefore varies between 1 and 15. When $L_{F0}/L_B = 0.5k$, k a positive integer, the polarised waves reflected by the gratings are aligned, and the PFS is close to 0 dB. In this case, the difference of propagation distance between the two reflected waves ($2L_F = 2L_{F0} + 2\Delta L_{max} \cos(2\pi ft)$) is close to a mulitple of L_B (For example see red dot in Fig. 3(b)). On the contrary, When $L_{F0}/L_B = 0.25(2k + 1)$, there exists (φ, χ) pairs which will induce reflected SOPs close to orthogonality since $2L_F$ is close to an odd multiple

Optics EXPRESS

of half the beat length. These (φ, χ) pairs will therefore generate a high PFS (For example see green dot in Fig. 3(b)).

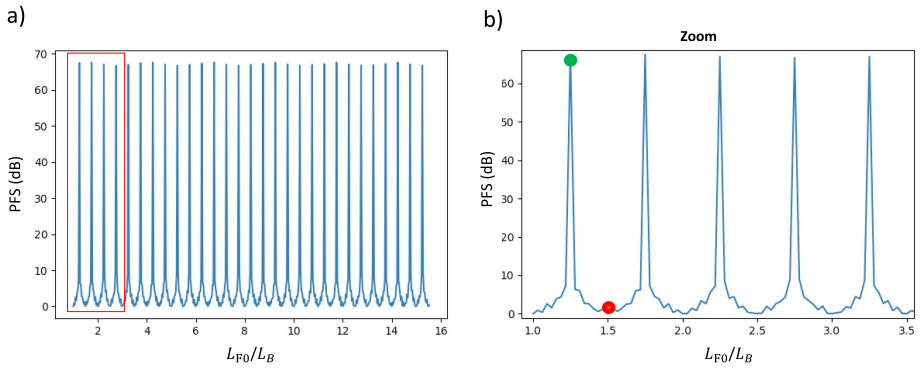

Fig. 3. Polarization fading sensitivity in unspun fibers: (a) PFS evolution as function of L_{F0}/L_B ranging from 1 to 15 and $\Delta L_{\max} = 1.68 \times 10^{-7}$ m, (b) zoom over [1,3.5].

Note that the case of unspun fibers studied in this section corresponds to the cases when a polarization maintaining fiber (PMF) or a single-mode fiber (SMF) (whith L_F much smaller than the coupling length [15]) section is placed between two successive FBGs. The only difference between the two cases is only the order of magnitude of the beat length: 1-50 m for SMFs and a few millimeters for PMFs. Since the horizontal axis of Fig. 3 is the ratio between L_{F0} and L_B, the figure is valid for both cases.

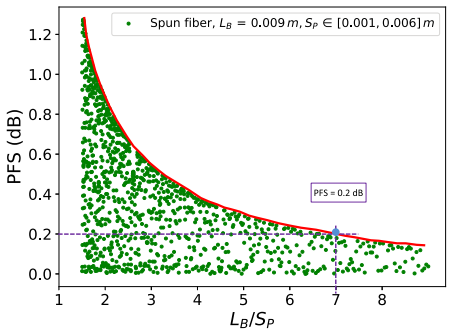

Fig. 4. Polarization fading sensitivity in spun fibers: PFS as a function of L_B/S_P (between 1.5 and 9) for $L_B = 0.009$ m, $L_{F0} = 1.24$ m, $\Delta L_{\max} = 1.68 \times 10^{-7}$m.

4.2. *Spun fibers case*

In order to mitigate the polarization effects in FBG-assisted φ-OTDR systems, it is interesting to substitute the unspun fiber placed between the FBGs for a spun fiber ($\xi \neq 0$). A spun fiber is characterized by its precursor beat length L_B and spun period S_P. Figure 4 depicts the PFS evolution as a function of L_B/S_P (between 1.5 and 9) for $L_B = 0.009$ m (case of hi-bi spun fibers), S_P from 0.001 to 0.006 m (ξ ranging from 1.047 10^{-3} to 6.283 10^{-3} rad/m) and $L_{F0} = 1.24$ m. The L_{F0} value of 1.24 m was chosen since it corresponds to the length used in the experimental work. One point on the figure corresponds to a specific L_B/S_P ratio (horizontal coordinate). To get that point, all the input SOPs are swept to find the PFS (vertical coordinate) using Eq. (1) and without changing L_B/S_P. It clearly appears that the general tendency is a decrease of the PFS when the L_B/S_P ratio increases (see the decreasing red curve on Fig. 4), demonstrating the effectiveness

Optics EXPRESS

of spun fibers in reducing polarization effects in an FBG-assisted φ-OTDR. In practice, for a target spatial resolution of the sensor (distance between two successive FBGs) and for a target PFS (depending of the desired polarization insensitivity level of the sensor), the simulation tool allows to find the required minimum L_B/S_P. For instance, a L_B/S_P ratio larger than 9 provides a PFS smaller than 0.15 dB for L_{F0} = 1.24 mm. Another example is the possibility to get a weak PFS of 0.2 dB for a L_B/S_P ratio equal to 7 and for a distance between two successive FBGs of 1.24 m (blue dot in Fig. 4), showing the possibility to perform polarization insensitive distributed vibration sensing with a spatial resolution of 1.24 m. A possible application is the monitoring of vibration frequencies of machines belonging to an industrial manufacturing chain.

5. Experimental results

The experimental setup presented in Fig. 5 is composed of the source, the sensing fiber, and the receiver. The light source consists of a narrow linewidth laser (NLL) emitting a highly coherent and continuous light with a linewidth of 0.1 kHz and a wavelength of 1552.5 nm. A pulse function generator (PG) enables to generate an electrical pulse signal sent to an acousto-optic modulator (AOM), which modulates the continuous lightwave to obtain a pulsed light with a repetition rate of 315 kHz and a pulse duration of 500 ns. The pairs of pulses are amplified by an erbium-doped fiber amplifier (EDFA), filtered by a bandpass filter (BPF, with a bandwidth of 1 nm around 1552.5 nm), and finally launched into the sensing fiber through the first port of an optical circulator. The backscattered/reflected light is guided to the receiver through port 3 of the circulator. The receiver is composed of an optical amplifier, two photodetectors (PD) with a transimpedance gain amplifier and a data acquisition card with 1 GS/s sampling rate. PD1 is used for synchronisation purposes and PD2 for detecting the reflected signal. Note that the choice of the laser linewidth results to a maximum distance between two successive FBGs. Twice the distance between two successive FBGs should be smaller than the source coherence length. For a 0.1 kHz linewidth, the coherence length is equal to about 600 km. If we move to a spectra width of 3 MHz (case of DFB laser), twice the distance between two successive FBGs should be smaller than 21 m.

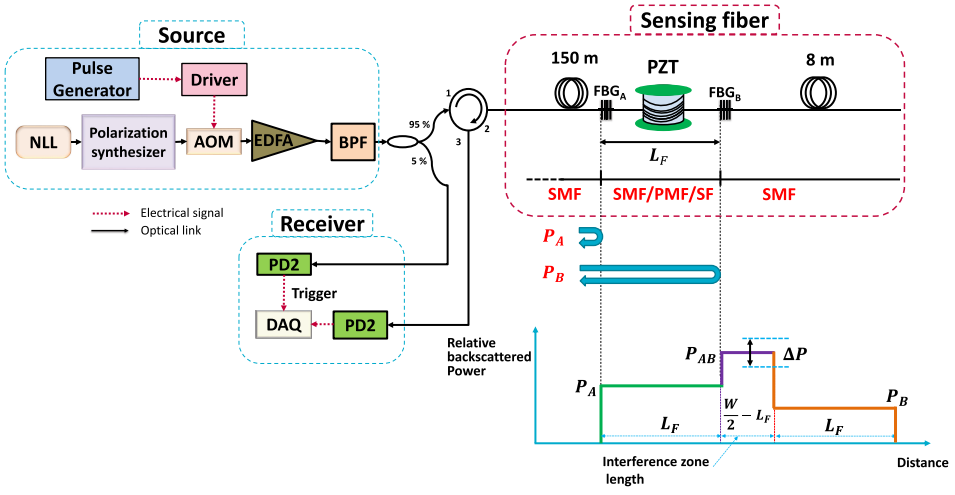

Fig. 5. Experimental setup

To study the polarization effects, two low reflectivity FBGs (1 %) have been inscribed in the sensing fiber. Both share globally the same characteristics, having a length of 4 mm, a center wavelength of 1552.5 nm and a 3 dB bandwidth of 0.2 nm. The grating pitch is equal to

Optics EXPRESS

536.42 nm. FBGs are separated by lengths of 40 m, 1.85 and 1.24 m for SMF, PMF and SF Fiber cases, respectively. The FBGs is preceded by a lead-in fiber spool of 150 m and terminated by a fiber spool of 8 m length.

The fiber section between the FBGs under test (SMF, PMF or spun fiber) is coiled around a cylindrical piezoelectric actuator having an outer diameter of 2.5 cm. The actuators are excited by a frequency generator with a sinusoidal signal having a peak-to-peak amplitude $V_{pp} = 44$ mV and a 10 kHz frequency. The polarization synthesizer placed after the source was configured to sweep all the possible SOPs (all the Poincaré sphere surface) over 3 s while keeping each SOP constant during 12 vibration periods of 10 kHz signal. This allows measuring the power variation ΔP corresponding to each SOP. The PFS can be determined after a complete SOP sweep. Note that the sensing fiber is covered by a plastic box to isolate it from the effect of lab environment (effect of the fans of various instruments, for instance).

Figure 6(a) shows the time-superposed traces measured by the φ-OTDR for one of the input SOP for a fiber section under test corresponding to a 40 m SMF28 . Considering the time-evolution of the power recorded at the interference position enables the measurement of $P_{AB}(t)$, and therefore ΔP. Figure 6(b) displays the interference signal $P_{AB}(t)$ at 195 m over a 0.7 ms time period for one SOP, and Fig. 6(c), its fast Fourier Transform (FFT). The 10 kHz component, corresponding to the piezoelectric actuator excitation frequency, can be clearly identified. The second harmonic at 20 kHz is also present due the nonlinear response of the direct detection scheme.

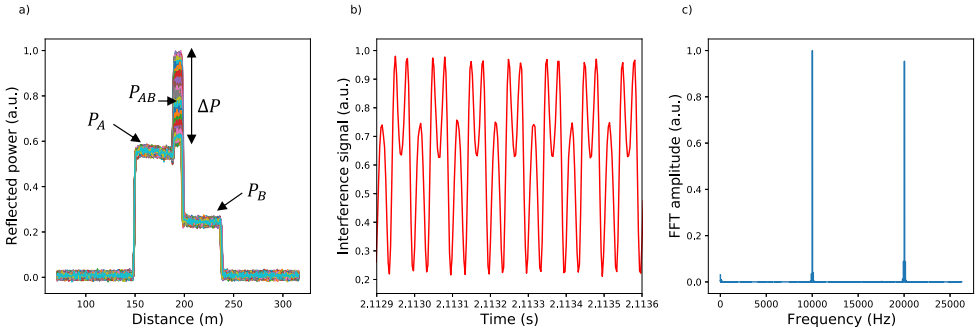

Fig. 6. (a) φ-OTDR traces (SMF28), (b) $P_{AB}(t)$ at 195 m and measured between 2.1129 and 2.1136 s for one SOP, and (c) FFT of $P_{AB}(t)$ at 195 m.

Figure 7 presents the detected interference signal $P_{AB}(t)$ while the polarization synthesizer sweeps all the possible input SOPs. V_{pp} (see section 4) was set so that $P_{AB}(t)$ covers all the response curve of the FBGs pair interference so that for a given SOP, the measured ΔP does not depend on the operating point (value of P_{AB} when vibrations are not applied). In zooms 1 and 2, the SOP change happening every 1.25 ms can be identified. For every SOP, ΔP is determined as shown in Zoom 3. As expected, ΔP varies with the SOP. By measuring ΔP as function of the SOP, ΔP_{max}, and ΔP_{min} then, the PFS can be calculated.

For two different cases of unspun fiber (SMF with length shorter than the coupling length and PMF), the corresponding PFSs were measured. Figure 8(a) presents a set of measured PFSs determined for an SMF28 wrapped around the PZT. The measurement was repeated 40 times. The mean PFS is $\mu_{SMF} = 5.20$ dB with a standard deviation of 0.06 dB. A good reproducibility was therefore obtained. In order to compare the experimental and numerical results, simulations were carried out with the L_B and L_{F0} values of the experiment. Figure 8(b) presents the simulated evolution of PFS as a function of L_{F0}/L_B between 12 and 16. The yellow zone represents the confidence interval for the L_{F0}/L_B ratio determined based on the measurement uncertainties of the fiber length between the FBG pair ($L_{F0} = 39.59 \pm 0.013$ m) measured with a photon-counting

Optics EXPRESS

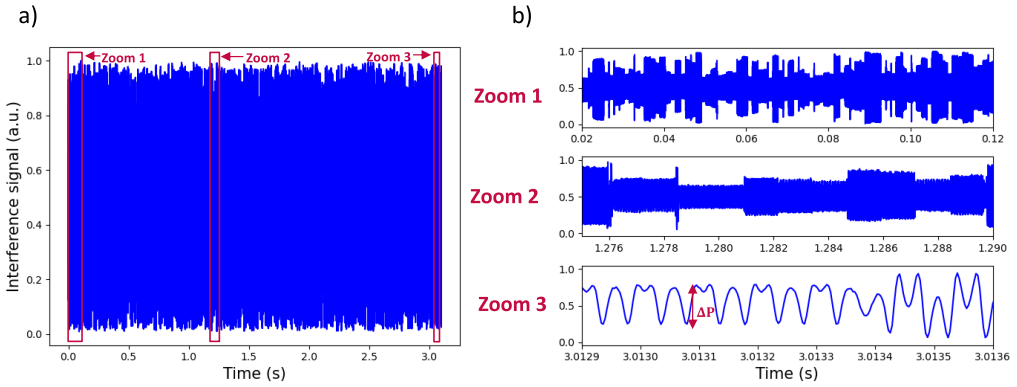

Fig. 7. Polarization effects and vibrations (SMF28): (a) $P_{\mathrm{AB}}(t)$ at 195 m measured over 3 s for all possible SOPs, and (b) zoom 1 over [0.02,0.12]s, zoom 2 over [1.275, 1.290] and zoom 3 over [3.0129, 3.0136]s

OTDR [28], and the beat length ($L_B = 2.764 \pm 0.115$ m) measured with a Polarization-OFDR [29]. The experimental PFS value is within the range provided by the simulation results.

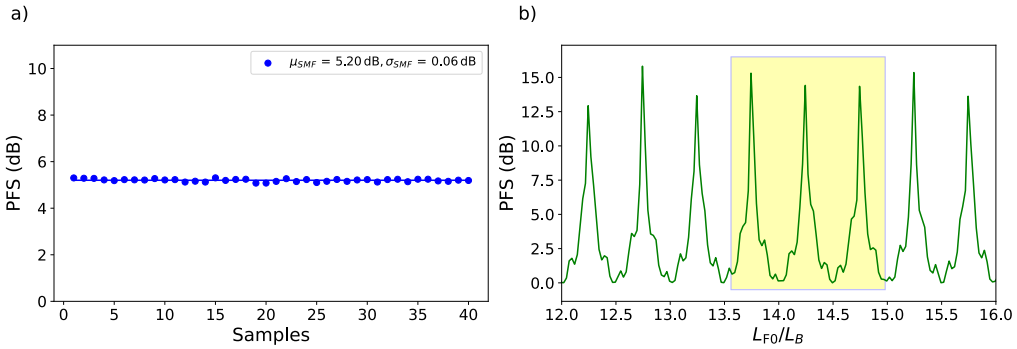

Fig. 8. Polarization effects and vibrations in SMF: (a) measured PFS for $L_B = 2.764$ m and $L_{\mathrm{F0}} = 39.59$ m, and (b) simulated PFS over L_{F0}/L_B

PFS measurements were then performed for an unspun PMF. We took 6 samples of different lengths from the same spool. The lengths L_{F0} and the measured PFS are displayed in Table 1. We can notice that the obtained PFS value strongly varies with the PMF length. Figure 9 presents the simulated evolution of PFS as a function of L_{F0}/L_B ratio between 570 and 635. The yellow zone ([596.3, 613.7]) represents the confidence interval for the L_{F0}/L_B ratio determined from the measurement uncertainty of the fiber length L_{F0} (±0.001 m), and the beat length ($L_B = 0.003$ m obtained from the datasheet). It clearly appears that the PFS value depends strongly on L_{F0}, which is in agreement with the large panel of measured PFS (see Table 1).

Table 1. PMF lengths used in the experiment and the measured PFSs

L_{F0} [m]	1.84	1.83	1.82	1.81	1.80	1.79
PFS [dB]	1.08	10.77	1.20	9.01	3.35	8.77

Note that for a given L_B, the uncertainty on the L_{F0} value does not allow a quantitative comparison with the PFS obtained by simulation for a specific L_{F0}/L_B ratio. The 1 mm

Optics EXPRESS

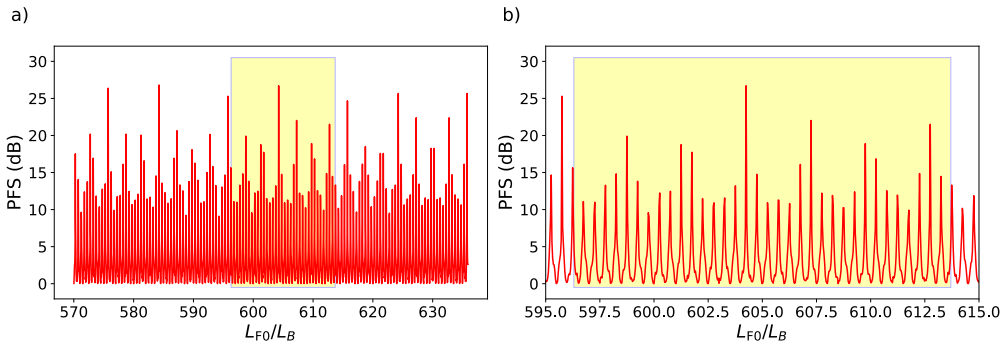

Fig. 9. Simulated PFS over L_{F0}/L_B for PMF with $L_B = 3$ mm: (a) $L_{F0}/L_B \in [570, 635]$, (b) Zoom inset: $L_{F0}/L_B \in [595, 615]$.

measurement uncertainty is indeed not small enough compared to the beat length (2.764 m and 3 mm for the SMF and PMD case, respectively).

Figure 10 presents measured PFSs for a spun fiber characterized by $L_B = 9.43$ mm, $S_P = 4.8$ mm and $L_{F0} = 1.24$ m. Figure 10(a) shows 40 successive measurements for the same configuration. The average PFS obtained was $\mu_{SF} = 0.8$ dB with a standard deviation of 0.02 dB, showing again a good reproducibility.

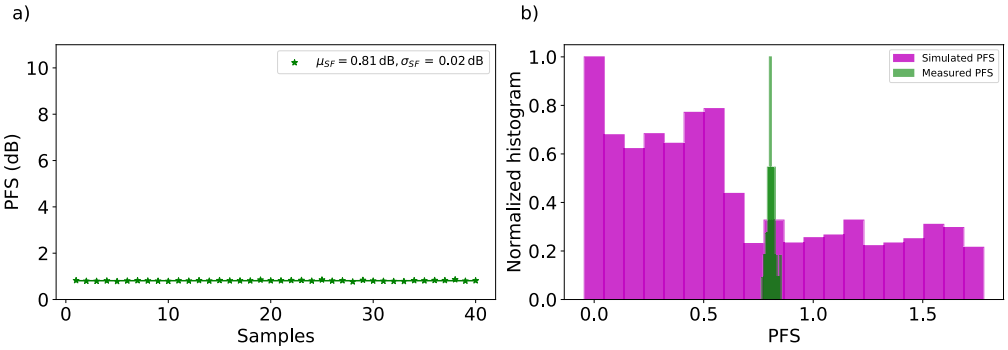

Fig. 10. Polarization effects and vibrations in SF: (a) measured PFS for $L_B = 9.43$ mm, $S_P = 4.8$ mm and $L_{F0} = 1.24$ m, and (b) simulated PFS over L_{F0}/L_B

Figure 10(b) displays the normalized histogram of simulated PFS (Montecarlo simulations) when considering the uncertainties on L_{F0} and L_B using uniform statistical distributions. The uncertainty on L_{F0} was again ±1 mm and the uncertainty on the beat length was calculated from the uncertainties on the circular beat length ($L_C = 75.2 \pm 0.31$ mm) and the spun period ($S_P = 4.8 \pm 0.048$ mm) provided by the manufacturer using the following formula [30]:

$$L_B = \frac{S_P}{\sqrt{(\frac{S_P}{L_C} + 2)^2 - 4}} \tag{16}$$

and results in a beat length uncertainty of $[9.36, 9.49]$ mm. The range of measured PFS is also presented in Fig. 10(b) (green histogram). The measured PFSs are the range of the simulated values. The triple (L_B, S_P, L_{F0}) used in the simulation that provided the closest value to the mean experimental PFS is (9.392 mm, 4,783 mm, 1,239591 m). Note that the PFS obtained for spun fibers are much smaller than the values obtained for SMF and PMF fibers, confirming the strong mitigation of polarization effects when using spun fibers.

Optics EXPRESS

6. Conclusion

In this work, a simulation tool was developed to analyze the polarization effects in FBG-assisted φ-OTDRs for both unspun and spun fibers. A piezo transducer (PZT transducer) was considered to simulate vibration between two successive FBGs. The numerical results showed that for the unspun fiber case, the PFS strongly depends on the ratio between the distance separating two consecutive FBGs and the beat length. The simulation work also quantified the mitigation effect of polarization fading when using spun fibers. PFS values as small as 0.2 dB can be reached when using a typical hi-bi spun fiber.

The numerical analysis was followed by an experimental study. An experimental setup was developed to measure the PFS for several fiber types. The obtained results qualitatively agreed with the numerical data.

Practically, the described simulation procedure provides a way to develop a tool to quantify the polarization fading sensitivity of an FBG-assisted direct detection φ -OTDR for a given configuration (type of fiber used between two consecutive FBGs, type of FBGs, type of vibration transduction) and is therefore helpful for the sensor design. Note that the simulation procedure could be upgraded to a coherent detection scheme if the corresponding layout is implemented in the simulation tool. The analysis performed in this paper, limited to the direct detection scheme, could for instance be useful in the frame of long-distance sensing when the cost of the interrogator is critical. A practical example is passive optical network monitoring (detection of moving fiber cable section within the network), for which the distance between the interrogator (located in the Central Office, CO) and the fiber ends of the tree-like structure can reach 20 km. In this context, it will be beneficial to use a DFB laser already installed in the CO to reduce the cost of the sensing system. Such optical sources do not provide a sufficient coherence length to use a coherent φ-OTDR interrogator. A direct detection should therefore be implemented, and a polarization diversity coherent detection scheme cannot be used to compensate the polarization fading. In this case, the study described in this paper allows to quantify the issue and to facilitate the design of a mitigation strategy.

Disclosures. The authors declare no conflicts of interest.

Data availability. Data underlying the results presented in this paper are not publicly available at this time but may be obtained from the authors upon reasonable request.

References

1. Y. Lu, T. Zhu, L. Chen, *et al.*, "Distributed vibration sensor based on coherent detection of phase-OTDR," J. Lightwave Technol. **28**(22), 3243–3249 (2010).
2. J. C. Juarez, E. W. Maier, K. N. Choi, *et al.*, "Distributed fiber-optic intrusion sensor system," J. Lightwave Technol. **23**(6), 2081–2087 (2005).
3. Y.-X. Bai, T.-T. Lin, and Z.-C. Zhong, "Noise reduction method of ϕ-OTDR system based on EMD-TFPF algorithm," IEEE Sens. J. **21**(21), 24084–24089 (2021).
4. F. Peng, N. Duan, Y.-J. Rao, *et al.*, "Real-time position and speed monitoring of trains using phase-sensitive otdr," IEEE Photonics Technol. Lett. **26**(20), 2055–2057 (2014).
5. Z. Qin, L. Chen, and X. Bao, "Continuous wavelet transform for non-stationary vibration detection with phase-OTDR," Opt. Express **20**(18), 20459–20465 (2012).
6. H. F. Martins, S. Martin-Lopez, P. Corredera, *et al.*, "Distributed vibration sensing over 125 km with enhanced SNR using phi-OTDR over a URFL cavity," J. Lightwave Technol. **33**(12), 2628–2632 (2015).
7. G. Cedilnik, G. Lees, P. E. Schmidt, *et al.*, "Pushing the reach of fiber distributed acoustic sensing to 125 km without the use of amplification," IEEE Sens. Lett. **3**(3), 1–4 (2019).
8. Y. Shan, W. Ji, X. Dong, *et al.*, "An enhanced distributed acoustic sensor based on UWFBG and self-heterodyne detection," J. Lightwave Technol. **37**(11), 2700–2705 (2019).
9. C. Wang, Y. Shang, X.-H. Liu, *et al.*, "Distributed OTDR-interferometric sensing network with identical ultra-weak fiber bragg gratings," Opt. Express **23**(22), 29038–29046 (2015).
10. F. Zhu, Y. Zhang, L. Xia, *et al.*, "Improved ϕ-OTDR sensing system for high-precision dynamic strain measurement based on ultra-weak fiber bragg grating array," J. Lightwave Technol. **33**(23), 4775–4780 (2015).
11. V. de Miguel Soto, J. Jason, D. Kurtoğlu, *et al.*, "Spectral shadowing suppression technique in phase-OTDR sensing based on weak fiber bragg grating array," Opt. Lett. **44**(3), 526–529 (2019).

Optics EXPRESS

12. E. B. Kocal, M. Wuilpart, and K. Yüksel, "Analysis of crosstalk effects in phase-OTDR system using fiber bragg grating array," Opt. Fiber Technol. **75**, 103176 (2023).
13. M. Sagues, E. Piñeiro, E. Cerri, *et al.*, "Two-wavelength phase-sensitive otdr sensor using perfect periodic correlation codes for measurement range enhancement, noise reduction and fading compensation," Opt. Express **29**(4), 6021–6035 (2021).
14. W. Tomboza, S. Guerrier, E. Awwad, *et al.*, "High sensitivity differential phase otdr for acoustic signals detection," IEEE Photonics Technol. Lett. **33**(13), 645–648 (2021).
15. F. Corsi, A. Galtarossa, and L. Palmieri, "Polarization mode dispersion characterization of single-mode optical fiber using backscattering technique," J. Lightwave Technol. **16**(10), 1832–1843 (1998).
16. T. Woliński, P. Lesiak, and A. Domański, "Polarimetric optical fiber sensors of a new generation for industrial applications," Bulletin of the polish academy of sciences technical sciences pp. 125–132 (2008).
17. D. Chen, Q. Liu, X. Fan, *et al.*, "Distributed fiber-optic acoustic sensor with enhanced response bandwidth and high signal-to-noise ratio," J. Lightwave Technol. **35**(10), 2037–2043 (2017).
18. C. Dorize and E. Awwad, "Enhancing the performance of coherent OTDR systems with polarization diversity complementary codes," Opt. Express **26**(10), 12878–12890 (2018).
19. T. Zhang, J. Lv, W. Li, *et al.*, "Coded phase-sensitive otdr with delayed polarization multiplexing for a wfbg array," Opt. Express **31**(3), 3708–3718 (2023).
20. K. Yuksel, V. Moeyaert, M. Wuilpart, *et al.*, "Optical layer monitoring in passive optical networks (PONs): A review," in *proceeeding of ICTON 2008*, vol. 1 (IEEE, 2008), pp. 92–98.
21. R. C. Jones, "A new calculus for the treatment of optical systems. VII. properties of the N-matrices," J. Opt. Soc. Am. **38**(8), 671–685 (1948).
22. M. Wuilpart, "Rayleigh scattering in optical fibers and applications to distributed measurements," in *Advanced fiber optics: concepts and technology*, L. Thévenaz, (editor) (EPFL Press, distributed by CRC Press, 2011), chap. 2, pp. 207–262.
23. M. Wuilpart, M. Aerssens, A. Gusarov, *et al.*, "Plasma current measurement in thermonuclear fusion reactors using a photon-counting POTDR," IEEE Photonics Technol. Lett. **29**(6), 547–550 (2017).
24. M. Wuilpart and M. Tur, "Polarization effects in optical fibers," in *Advanced fiber optics: concepts and technology*, (EPFL Press (L. Thévenaz (editor), distributed by CRC Press, 2011), chap. 2, pp. 29–84.
25. T. Erdogan, "Fiber grating spectra," J. Lightwave Technol. **15**(8), 1277–1294 (1997).
26. P. Dandu, S. Kim, A. Gusarov, *et al.*, "Precursor beat length and spun period measurement of a spun fiber using polarization optical frequency domain reflectometry," Opt. Lett. **48**(2), 319–322 (2023).
27. R. I. Laming and D. N. Payne, "Electric current sensors employing spun highly birefringent optical fibers," J. Lightwave Technol. **7**(12), 2084–2094 (1989).
28. M. Wegmuller, F. Scholder, and N. Gisin, "Photon-counting OTDR for local birefringence and fault analysis in the metro environment," J. Lightwave Technol. **22**(2), 390–400 (2004).
29. L. Palmieri and A. Galtarossa, "Distributed polarization-sensitive reflectometry in nonreciprocal single-mode optical fibers," J. Lightwave Technol. **29**(21), 3178–3184 (2011).
30. J.-R. Qian, "A note on the beat length of spun linear birefringence fiber," Microw. Opt. Technol. Lett. **16**(4), 225–227 (1997).